RSC Advances

PAPER

View Article Online
View Journal | View Issue



Cite this: *RSC Adv.*, 2016, **6**, 104201

# Effects of temperature, pH and counterions on the stability of peptide amphiphile nanofiber structures†

Alper D. Ozkan, Ayse B. Tekinay,* Mustafa O. Guler* and E. Deniz Tekin*

Peptide amphiphiles are a class of self-assembling molecules that are widely used to form bioactive nanostructures for various applications in bionanomedicine. However, peptide molecules can exhibit distinct behaviors under different conditions, suggesting that environmental variables such as temperature, pH, electrolytes and the presence of biological factors may greatly affect the self-assembly process. In this work, we used united-atom molecular dynamics simulations to understand the effects of three counterions ($Na^+$, $Ca^{2+}$ at pH 7 and $Cl^-$ at pH 2) and temperature change on the stability of the lauryl-VVAGERGD peptide amphiphile self-assembly. This molecule contains a bioactive RGD peptide sequence and has been shown to support cellular adhesion and proliferation *in vitro*. A 19-layered peptide nanostructure, containing 12 peptide amphiphile molecules per layer, was previously shown to exhibit optimal stability and it was used as the model nanofiber system. Peptide backbone stability was studied under increasing temperatures (300–358 K) using the number of hydrogen bonds and root-mean-square deviations of nanofiber size. At higher temperatures, fiber disintegration was observed to be dependent on the type of counter-ion used for nanofiber formation. Interestingly, rapid heating to higher temperatures could sometimes reestablish the integrity of the nanofiber backbone, possibly by allowing the system to bypass an energy barrier and assuming a more thermodynamically stable configuration. As counterion identity was observed to exhibit remarkable effects on the thermal stability of peptide nanofibers, we suggest that these behaviors should be considered while developing new materials for potential applications.

Received 24th August 2016
Accepted 26th October 2016

DOI: 10.1039/c6ra21261a

www.rsc.org/advances



## Introduction

Peptide amphiphiles (PAs) are an important class of bioactive molecules that have the ability to self-assemble into high-aspect ratio nanofibers due to their noncovalent interactions such as electrostatic, van der Waals, hydrogen bonding, hydrophobic and aromatic (π–π stacking) interactions. In aqueous conditions, networks of PA nanofibers form gels that exhibit the potential to be used in tissue engineering and regenerative medicine[1–3] due to their biofunctionality, biocompatibility and biodegradability.[4–6] While the self-assembly mechanism is based on noncovalent interactions, it is also responsive to environmental factors such as temperature, pH and presence of enzymes.[7–12] The effects of temperature on the self-assembly mechanism of PA molecules were studied by Miravet *et al.* and other groups.[13–15] They observed a thermal transition from nanotapes at 293 K to micelles at higher temperatures (the transition temperature depends on the concentration) in self-assembly of PA palmitoyl-KTTKS. Similarly, Hamley *et al.*[16] observed a reversible thermal transition in the self-assembly mechanism of a designed PA, palmitoyl-KKFFVLK. They also discovered that a designed PA, which self-assembles into nanotubes and helical ribbons in aqueous solution at room temperature, takes the form of twisted tapes upon heating to 328 K, and nanotubes and helical ribbons reappear after re-cooling. A change in the pH can also affect the self-assembly mechanism of the PA molecules. Niece *et al.*[17] observed the nanofiber formation over a wide range of pH values with positively/negatively-charged PA molecules. The negatively charged PA molecules self-assemble at acidic pH, the positively charged PA molecules self-assemble at basic pH and oppositely charged PA molecules co-assemble at neutral pH. Toksoz *et al.*[18] also studied neutral/positively/negatively-charged PA molecules to understand the formation of nanofibers due to pH change or addition of electrolytes. Chen *et al.*[19] designed a series of pH-responsive PAs with the same length of alkyl chain ($C_{16}$), but differ in length of the alternating arginine and aspartic acid sequence. They demonstrated that changing pH allows

*Institute of Materials Science and Nanotechnology, National Nanotechnology Research Center (UNAM), Bilkent University, Ankara, 06800, Turkey. E-mail: atekinay@bilkent.edu.tr; moguler@unam.bilkent.edu.tr; edeniztekin@gmail.com*

† Electronic supplementary information (ESI) available: Observations on PA1 nanofiber structure under extended simulation periods, secondary structure and radius of gyration analyses of all three PA configurations, and hydrogen bond formation of PA2 nanofibers. See DOI: 10.1039/c6ra21261a

hierarchical self-assembly of PA molecules into micelles, fibers and packed fibers. Ghosh *et al.*[20] synthesized six different PA molecules that exist as either isolated PA or spherical micelles at pH 7.4 and self-assemble into fibers at pH 6.6, which emulates the acidic extracellular environment of tumor tissue. Dehsorkhi *et al.*[21] have studied the effects of pH change (at pH 2, 3, 4 and 7) on the self-assembly of palmitoyl-KTTKS. They observed that the self-assembled structures were changed form from tapes to twisted fibrils and back to tapes to spherical micelles with pH reduction. Deng *et al.*[22] designed a PA by attaching the lauric acid covalently to a fragment of the Aβ (lauryl-Aβ(11–17)) to study the conformational changes in the final self-assembled nanostructures by varying the pH values. At the same concentration (in 1.87 mM lauryl-Aβ(11–17)) solution, they observed tape-like nanofibrils at pH 3 and nanoribbons at pH 10. Guo *et al.*[23] showed that the lauryl-GAGAGAGY molecules, which were derived from silk fibroin, exhibited pH-sensitive assembly. When the value of pH decreases from 11 to 8, self-assembled nanostructures changed from nanofibers to nanoribbons (mostly parallel bundles of nanoribbons). Dagdas *et al.*[24] comprehensively studied the mechanical properties of the self-assembled lauryl-VVAGERGD molecules by altering the temperature and pH. The PA nanofibers were formed by using $Na^+$ coordination at pH 7, $Ca^{2+}$ coordination at pH 7 or H-coordination through the addition of HCl at pH 2. These formulations exhibited similar properties under SEM, TEM, AFM, FTIR and room-temperature circular dichroism (CD); however, a slight difference in temperature-dependent CD was noted between the $Ca^{2+}$-treated and the HCl-treated samples, which also displayed marked differences in temperature-dependent mechanical integrity under oscillatory rheology.

Experimental results have shown that tuning the self-assembly of the PA molecules by changing the environmental variables such as temperature and pH greatly affects the morphology of the resulting aggregate nanostructures. Even though the role of environmental variables on morphological properties of resulting nanostructures has been investigated experimentally, it has not been sufficiently studied theoretically. In the literature, there are some simulation studies about the temperature change, but studies about the effects of pH on nanofiber formation are scarce. Because there is a limitation on the pH-dependent simulations, it cannot be investigated by standard explicit solvent molecular dynamics (MD) simulations since they are constant-proton algorithms.

Cote *et al.*[25] used the multiscale MD simulations to investigate the pH-dependent self-assembly of palmitoyl-IAAAEEEE based fibers. Coarse-grained discontinuous MD was used for kinetic details, and all-atom constant pH molecular dynamics (CpHMD) simulations were used for thermodynamics features. In the CpHMD simulations, the alkyl tails were excluded and the initial structure was prepared as a tetramer putting four PA molecules in a parallel β-sheet conformation with protonated Glu residue. After 100 ns standard all-atom MD with fixed protonation states, the final structure was taken as an input for the CpHMD

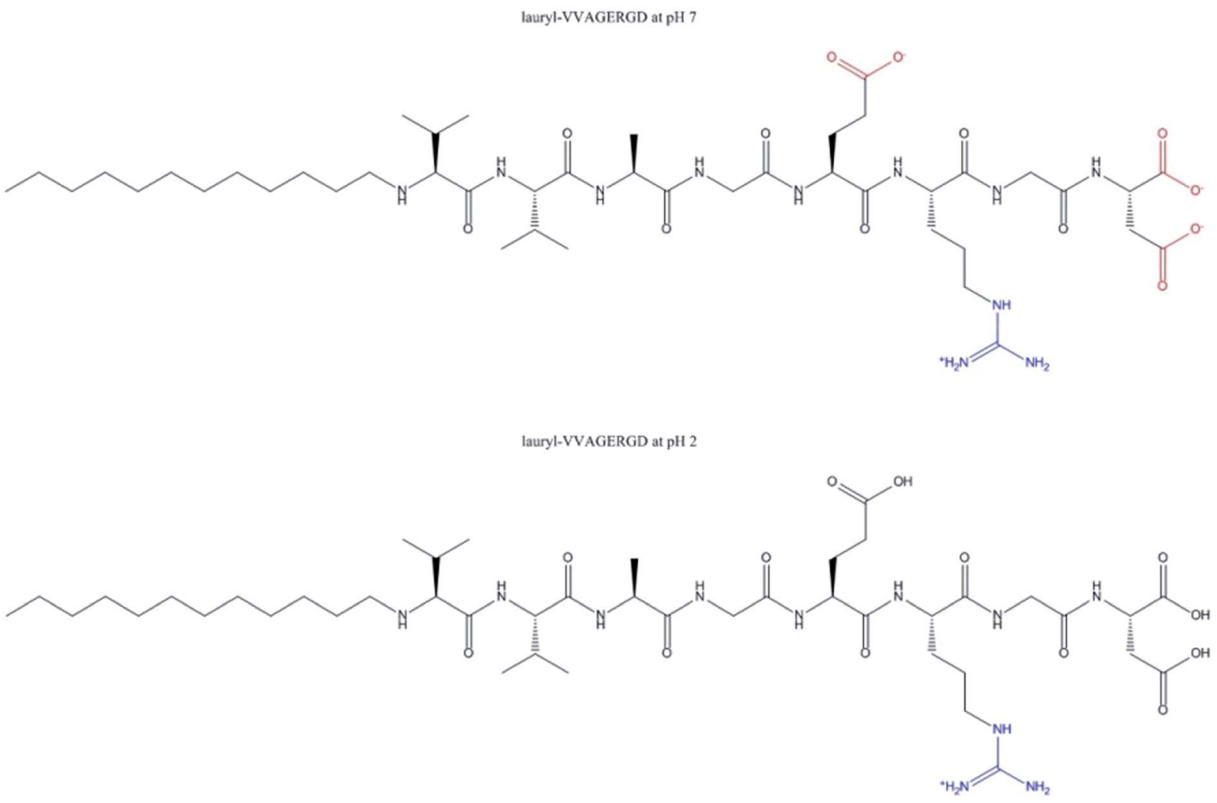


Fig. 1 Chemical structures of lauryl-VVAGERGD at pH 7 and pH 2.

 

simulations. To quantitatively predict the pH-dependent mechanism, they calculated the total number of backbone hydrogen bonds as a function of pH and observed the transition between the random coil and the β-sheet in range of pH 6–7. Fu *et al.*[26,27] observed a large number of different nanostructures through the self-assembly of model PA, palmitoyl-VVVAAAEEE, by changing the temperature (ranging from $T = 260$ K to $T = 550$ K) at distinct hydrophobic interaction strength by discontinuous MD simulation algorithm. In a previous study by this group,[27] the resulting self-assembled nanostructures were observed to depend on the electrostatics and the temperature with the same PA molecules. Specifically, nanofibers occurred at the temperature range of 376–414 K (moderate region) with weak electrostatic strength, whereas spherical micelles were observed at the temperatures 300–338 K (low region) and again with weak electrostatic strength.

Recently,[28] MD simulations of multiple PA nanofibers revealed the structural features and the role of molecular interactions on their stability. In particular, the number of the PA molecules on each layer was found to determine the overall stability of the nanofiber. 7, 9 and 12-layered nanofibers were found to trigger the formation of spherical micellar assemblies, while 13, 14, 16 and 19-layered nanofibers supported the formation of nanofibers after 50 ns of simulation. Other nanofibers, consisting of 17, 18, 20 and 21 layers, were unable to support the formation of stable structures and disassembled within 1 ns of simulation time. Both hydrophobic (VVAG) and hydrophilic (ERGD) sections of the model PA were found to play key roles in the assembly process, with VVAG–VVAG, D-$Na^+$ and E-R interactions serving to organize the aggregation of the peptide molecules. The 19-layered nanofiber, where each layer was composed of 12 PA molecules,[29] was found to be the most stable configuration among the simulated structures and also, the diameter of nanofiber was found to be 8.4 nm, which is in close agreement with experimental observations.[5,30] For these reasons, the 19-layered system was ultimately chosen as the model of interest for further simulations.

In this work, we studied the effects of temperature, charge neutralization with different ions ($Na^+$, $Ca^{2+}$, $Cl^-$) and PA molecules at different pH (pH 7 and pH 2) on preassembled, cylindrical PA nanofibers. Lauryl-VVAGERGD molecule was chosen as the model molecule, and contains a bioactive RGD peptide sequence which has been shown to support cellular adhesion and proliferation *in vitro*, and of which thermal behavior was investigated experimentally.[24] $Na^+$ and $Ca^{2+}$ mediated assemblies were modelled at pH 7, as is the assumed standard of united-atom MD, while the effects of pH on peptide aggregation behavior was investigated through the inclusion of additional $H^+$ ions within the initial PA structure. As noted above, this path was taken because standard explicit solvent MD simulations are constant-proton algorithms and cannot directly simulate molecular assembly at different pH values (simulation details are provided in the Methods section). In addition, PA nanofiber behavior was not investigated under basic pH because negatively-charged PAs do not self-assemble under basic conditions due to electrostatic repulsion.

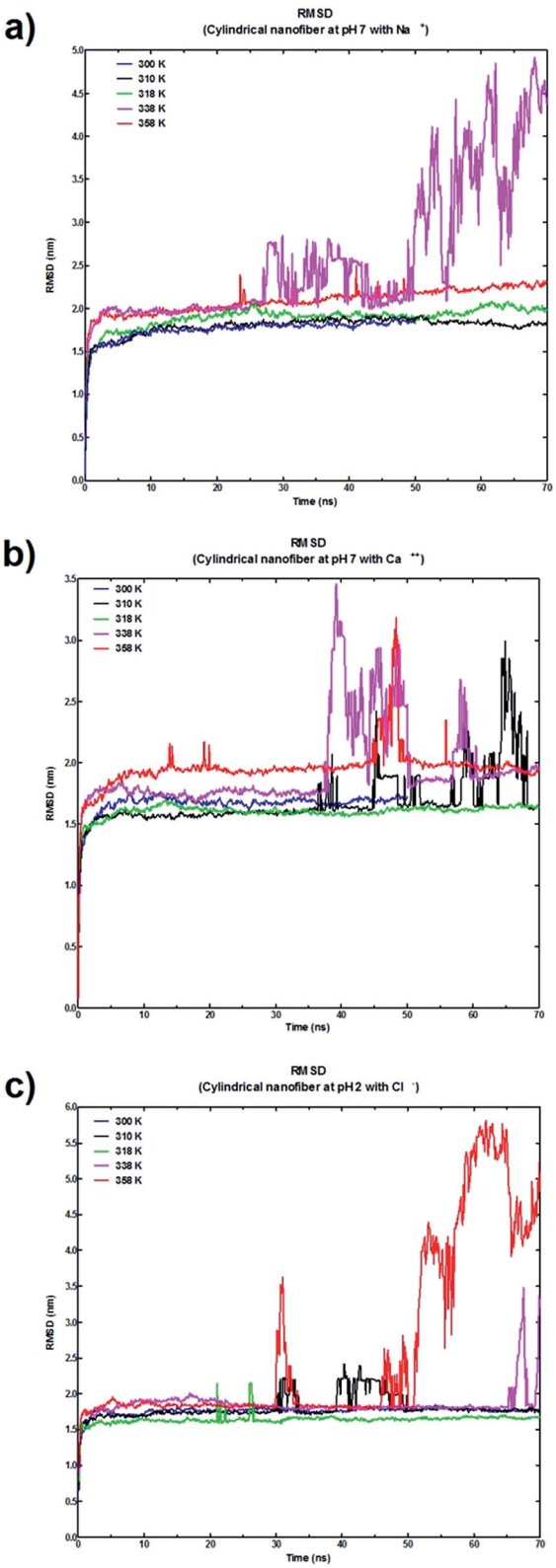


Fig. 2 RMSD graphs of (a) PA1, (b) PA2, and (c) PA3 nanofibers. RMSD values greater than 2 nm are assumed to represent nanofiber disintegration, which typically occurs at 338 K or 358 K.

# Methods

### Simulation details

The lauryl-VVAGERGD nanofibers were formed under three different formulations; PA molecules at pH 7 with $Na^+$ ions (PA1); PA molecules at pH 7 with $Ca^{2+}$ (PA2) and PA molecules at pH 2 with $Cl^-$ ions (PA3) (Fig. 1). In PA1 and PA2, the total net charge is −2 with charges Glu (E) = −1, Arg (R) = +1, Asp (D) = −2 (including the end-chain $COO^-$ = −1). As a result, the excess of negative charge on the nanofiber was neutralized by adding a sufficient number of $Na^+$ ions to the PA1 nanofiber and $Ca^{2+}$ to the PA2 nanofiber. To represent pH 2 in PA3, Glu (E) and Asp (D) side chains were protonated with Glu (E) = 0, Arg (R) = +1 and Asp (D) = 0, so the total net charge of the PA3 molecule is +1. Sufficient number of $Cl^-$ was added to the PA3 nanofiber to make it neutral. Each structure was immersed in a rhombic dodecahedron box of SPC type water molecules.[31] Then, energy minimization was carried out to the solvated-electroneutral systems with the steepest-descent algorithm to get suitable starting conformations. Each system was equilibrated with NVT and NPT (100 ps for each) prior to a 70 ns MD production run with GROMACS 4.5.6.[32] GROMOS 53a6 (ref. 33) force field combined with Berger lipid parameters[34] was used to represent the PA molecules. Initial velocities were assigned from a Maxwell–Boltzmann distribution. To get the time evolution of the PA nanofibers (the trajectories), Newton's equation of motion was solved numerically using the Leap-Frog algorithm with a 2 fs integration time-step. The linear constraint solver (LINCS) algorithm[35] was applied to all bonds containing hydrogen bonds. In calculating the electrostatic interaction, the Particle Mesh Ewald (PME) method[36] was used and a 1.0 nm cut-off was set for the calculation of the van der Waals interactions. Simulations were performed with periodic boundary conditions in all directions at constant temperature and pressure. The temperature was kept constant at various temperatures using a velocity rescaling thermostat[37] with two coupling groups (PA and non-PA groups) and with a coupling time constant of 0.1 ps. The pressure was maintained at 1 bar using an isotropic Parrinello–Rahman barostat[38] with a coupling time constant of 2.0 ps. Coordinates and energies were saved at every 10 ps for the trajectory analysis. The snapshots were obtained using the visual molecular dynamics (VMD) software.[39]

For all three formulations, MD simulations were carried out around the room temperature (300 K) and at variable temperatures (310 K (body temperature), 318 K, 338 K and 358 K) for 70 ns. According to the results of these simulations, to better understand the temperature-dependence of PA1 nanofiber, two more simulations were carried out: first, the final configuration at the end of the 70 ns simulation at 338 K of the PA1 nanofiber was extracted to heat it up to 358 K. Second, temperature was raised at every 20 ns steps, from 300 K to 358 K. In each case, the self-assembly simulations were started from a configuration in which 228 PA molecules were put to form cylindrical nanofibers as described previously by Tekin.[28,29]

# Results

In this work, an extensive MD study of the temperature-dependent trajectory of the PA-based cylindrical nanofibers

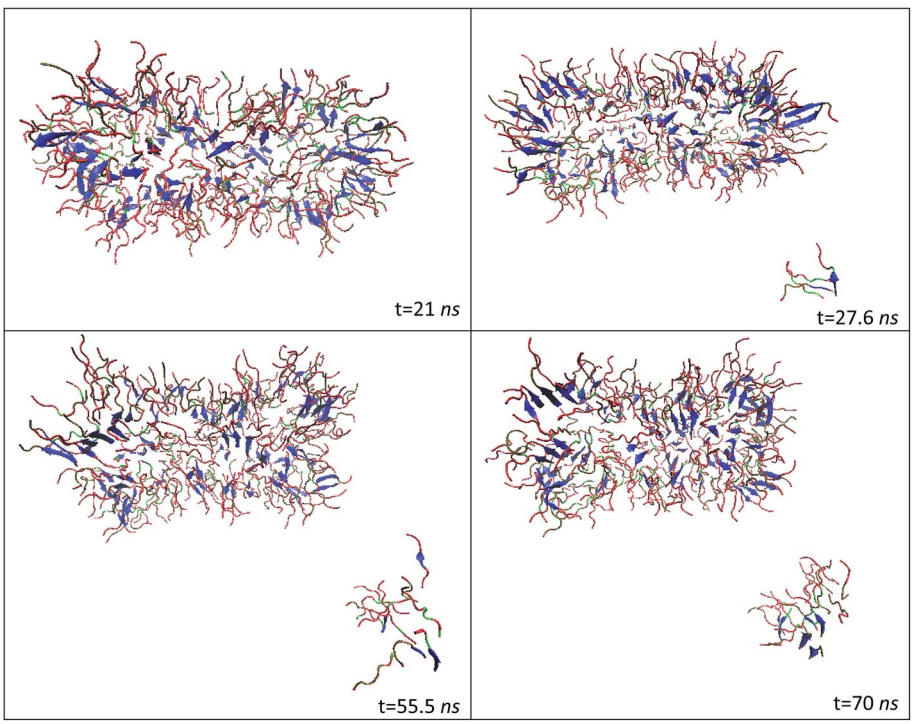


Fig. 3 Snapshots of PA1 nanofiber at 338 K. The nanofiber was observed to lose its cohesion after 55 ns, and the peptide assembly eventually split into two.

 

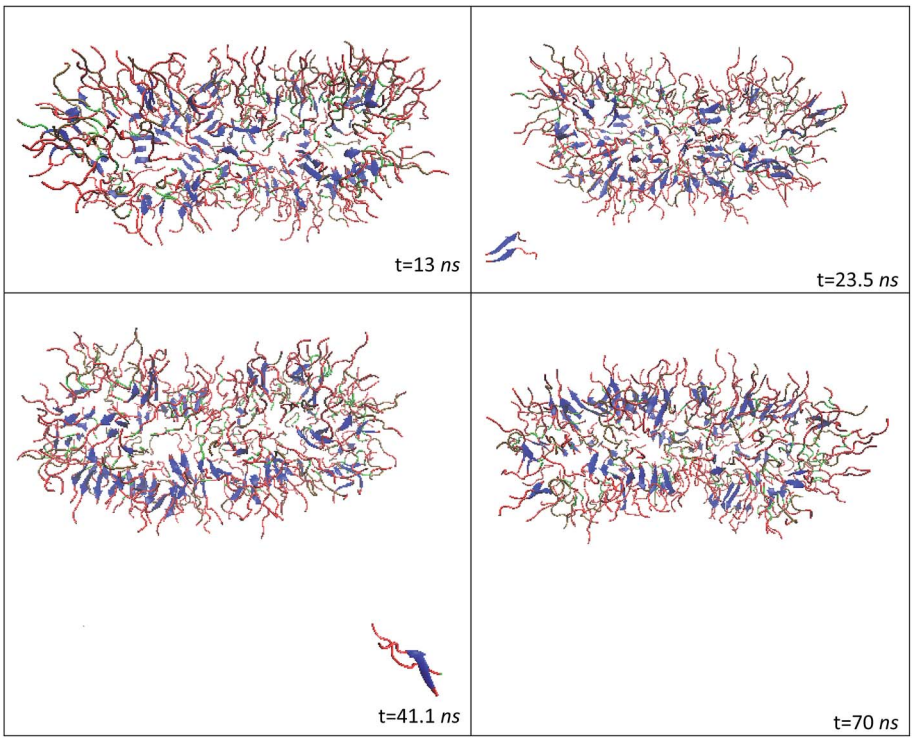


Fig. 4 Snapshots of PA1 nanofiber at 358 K. Despite the departure of some PA molecules from the network, the system retained its overall structure.

prepared at pH 7 and pH 2 with different charge neutralizing ions is presented. Stability of the PA1, PA2 and PA3-based cylindrical nanofibers at five different temperatures was analyzed using the RMSD of the backbone atoms comparing the energy minimized configuration of the initial nanofiber and the equilibrated system after 70 ns (Fig. 2a–c). For all three nanofibers at 300 K and 318 K, RMSD values were below/around 2 nm and the structures maintained their cylindrical form, and they were stable under these conditions. PA1 and PA3 nanofibers were observed to be stable at the physiological temperature (310 K), with the exception of a minor, temporary increase in RMSD values (between 39.3 ns and 46.5 ns) for PA3 nanofibers, which was observed not to result in fiber disintegration (see Fig. SI-1†). However, PA2 nanofiber was not stable after 45 ns, the RMSD is momentarily above 2.0 nm, and then goes down below 2 nm, and after that the RMSD oscillates up and down. When the temperature increased to 338 K and to 358 K, some unexpected results appeared.

As shown in Fig. 2a, although the RMSD of the PA1 nanofiber at 338 K was greater than 2.0 nm after 27 ns, the structure retained its cylindrical form. However, the PA nanofiber started to lose its cylindrical form and split into two after 55 ns (Fig. 3).

As also shown in Fig. 2a, at 358 K after 22 ns, the RMSD of the structure was slightly above 2 nm and also reached some peak values. At these values, some PA molecules were breaking away from the nanofiber form (see Fig. 4). However, disintegration was not observed at 358 K unlike the case we saw at 338 K.

Since disintegration of the nanofiber could be expected as the temperature increases, two more simulations were performed to determine the reason behind the absence of nanofiber disassembly at 358 K. In the first simulation (simulation-1), the configuration of the PA1 nanofiber after 70 ns of simulation at

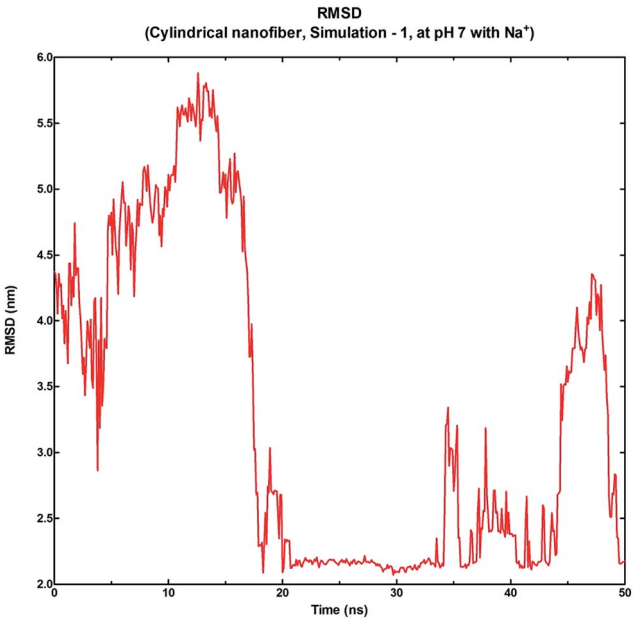


Fig. 5 RMSD graph of simulation-1 for the PA1 nanofiber. The initial structure was taken from 338 K and heated up to 358 K. The peptide system regained its structure in the 20–35 ns interval, but exhibited fluctuations in the nanofiber radius after this time period.

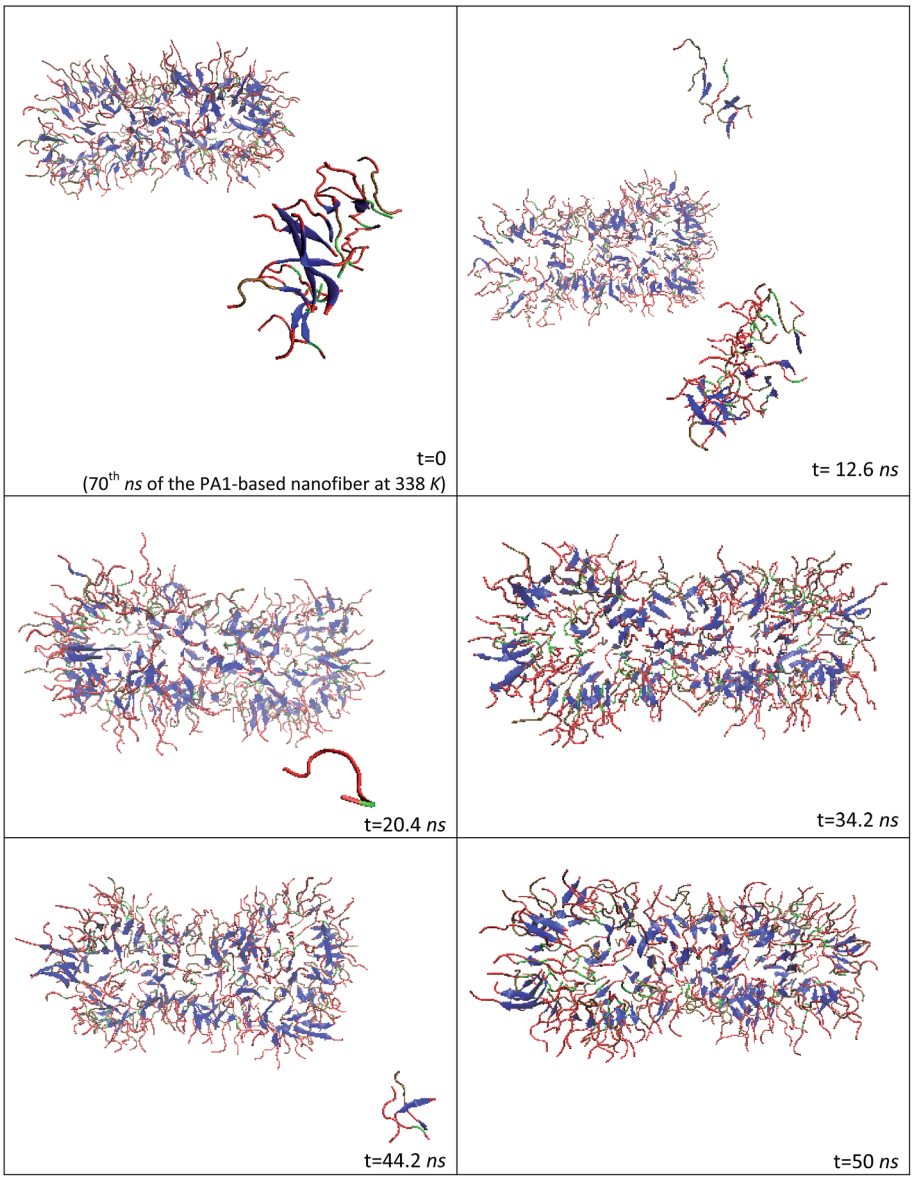


Fig. 6 Snapshots of simulation-1 for PA1 nanofiber. As with the RMSD results, the snapshots suggest that the peptide system reassembled after 20 ns of heating.

338 K was extracted and heated to 358 K. In the second simulation (simulation-2), temperature was raised in 20 ns intervals, from 300 K to 358 K.

In simulation-1, the starting structure was in two pieces, Fig. 5 and 6, (RMSD is around 4.4 nm) and they went back together after 18.3 ns creating its initial cylindrical form (RMSD is about 2 nm). However, after 34.2 ns, the RMSD increased again, but there was no disintegration. In fact, this result was consistent with the simulations at 338 K and 358 K.

In simulation-2, the temperature of the system was increased from 300 K to 358 K gradually at each 20 ns. The RMSD (Fig. 7) values started fluctuating after 97 ns, and the structure began to crumble after 112 ns, which corresponds to 358 K (Fig. 8). In other words, we did not observe any disintegration at 338 K unlike the case of directly heating up of the PA1 nanofiber to 338 K. Since the 20 ns simulation at 338 K might not have been sufficient to observe disintegration, we extended this part of the simulation to 70 ns. This extended simulation did not change the status, that is, the RMSD values were below 2 nm during the simulation time, confirming the stability of the structure (Fig. SI-2†).

In addition, to understand the results of simulation-2; we also wondered whether disintegration occurs if we extend the simulation for the PA1 nanofiber at 358 K for a total of 120 ns; however, the results did not change much (see Fig. SI-3†).

The RMSD value of the PA2 nanofiber at 338 K was above 2.5 nm after 38 ns and some of the PA molecules broke away from the nanofiber (Fig. 2b and 9). But between 51 and 57 ns, the structure took the form of a cylinder, disintegrated, and

 

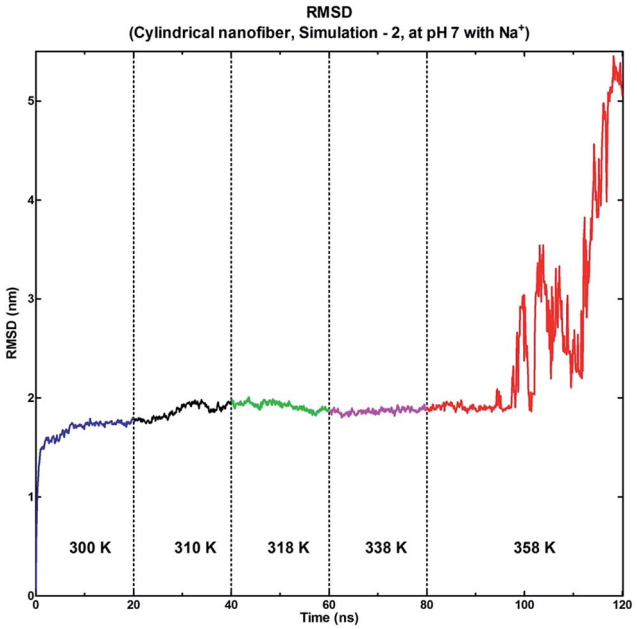


Fig. 7 The RMSD graph of the gradually-heated PA1 nanofiber from 300 K to 358 K (simulation-2). Complete disassembly of the nanofiber system was observed only at 358 K.

eventually reassumed its cylindrical shape between 60.7 and 70 ns (RMSD < 2.0 nm).

At 358 K, although there were break-ups between the 45.4–49 ns, it can be concluded that the structure kept its initial structure (Fig. 2b and 10).

When we compared the simulations of the PA1 and PA2 nanofibers at 338 K and 358 K, we observed that the change in the RMSD at 338 K was greater than the change in the RMSD at 358 K for both structures. However, during the simulation of the PA2 nanofiber, there was an instability (disintegration – cylindrical nanofiber – disintegration and the pattern repeats) while in the PA1 nanofiber if the structure disintegrated, it could not take the form of a cylinder again. In addition, during the simulation of the PA2 nanofiber at 310 K, large values and fluctuations in the RMSD graph were not expected. We would expect that the RMSD value should be around 2 nm at such a low temperature. So we can say that systems with excess negative charge should be neutralized by $Na^+$ ions instead of $Ca^{2+}$ ions. Further information about the PA2 nanofiber can be found at the ESI (SI-5 and SI-7†).

MD force fields are often amended with parameter sets for specific ions and molecules (and especially multivalent ions) to ensure that the simulated behavior accurately represents the experimental observations. Merz and Li have shown that the 12-6 Lennard-Jones (LJ) model can be modified with an additional term ($1/r^4$) for the development of parameter sets capable of representing a full range of divalent ion behaviors in several force fields, such as AMBER, CHARMM, and OPLS-AA.[40,41] Mamatkulov *et al.* also developed a set of parameters for divalent ions for AMBER, CHARMM and GROMOS force fields,[42] and Bergonzo *et al.* likewise compared the effectiveness of several parameter sets in simulating the behavior of Mg-linked RNA stem loops.[43]

In the RMSD analysis of PA3 nanofiber at 338 K (Fig. 2c), even if the PA3 nanofiber at 338 K (Fig. 11) started to disintegrate towards the end of the simulation, at 358 K (Fig. 12) the structure was broken in to 3 parts (RMSD was above 3.5 nm and above) and it lost its cylindrical form.

The PA1 nanofiber disintegrated around 338 K, but keeps its initial form at 358 K. On the other hand, the PA3 nanofiber disintegrated around 358 K. Radius of gyration analysis was also performed to further support our RMSD results as a measure of convergence. Fiber compactness was found to correlate strongly with backbone fluctuations, suggesting that our conclusions based on RMSD values were reliable (SI-8†).

The secondary structure content of each nanofiber as a function of time at different temperatures was defined by the Dictionary of Secondary Structure of Proteins (DSSP) program designed by Kabsch and Sander[44] (Fig. SI-4 and SI-6†). At each temperature, all three PA nanofibers had random coils as their dominant secondary structure; at the ranges of 69–65%; 63–67% and 59–53% for PA1, PA2 and PA3, respectively. The β-sheets were the second adopted structures by all nanofibers, ranging between 9–11% for the PA1 nanofiber, 9–11% for the PA2 nanofiber and 15–21% for the PA3 nanofiber. Thus, the PA molecules prepared at low pH had more β-sheet (or less random coil) structures at each temperature, suggesting that acid-mediated self-assembly results in more organized structures. In addition, as seen from the Table 1, the percentage of β-sheet decreased in the case of disintegration.

Hydrogen bonds between the PA molecules were analyzed by assuming the existence of the bond for the O–H distances of 0.35 nm or smaller, and an OHN angle of 30 degrees or less (Fig. 13a–d). There were more (albeit slightly) H-bonds during the simulation time in the PA3 nanofiber compared to the PA1 nanofiber during the simulation time at each temperature. The same result was also obtained from the DSSP analysis as noted above: the ratio of β-sheets in the PA3 nanofiber during the simulation time at each temperature was greater than the one in the PA1 nanofiber (see Table 1). In general, there was an increase in the number of H-bonds with increasing temperature.

## Discussion

The RMSD analyses suggest that temperature increase results in the loss of nanofiber structure, with the 338 K and 358 K simulations in particular demonstrating that higher temperatures compromise the compactness of the peptide backbone. The fact that the PA1 nanofiber at 338 K simulation suggested the total disassembly of the nanofiber also merits some note, since a similar effect was not observed in the 358 K results (see Fig. 2a). Proteins and peptides often exhibit irreversible changes in their assembly characteristics following heating, which usually (but not necessarily) accompany loss of biological function and drive the structure to a more stable equilibrium following the disruption of electrostatic interactions.[45] Therefore, the structure at 338 K may possibly represents an

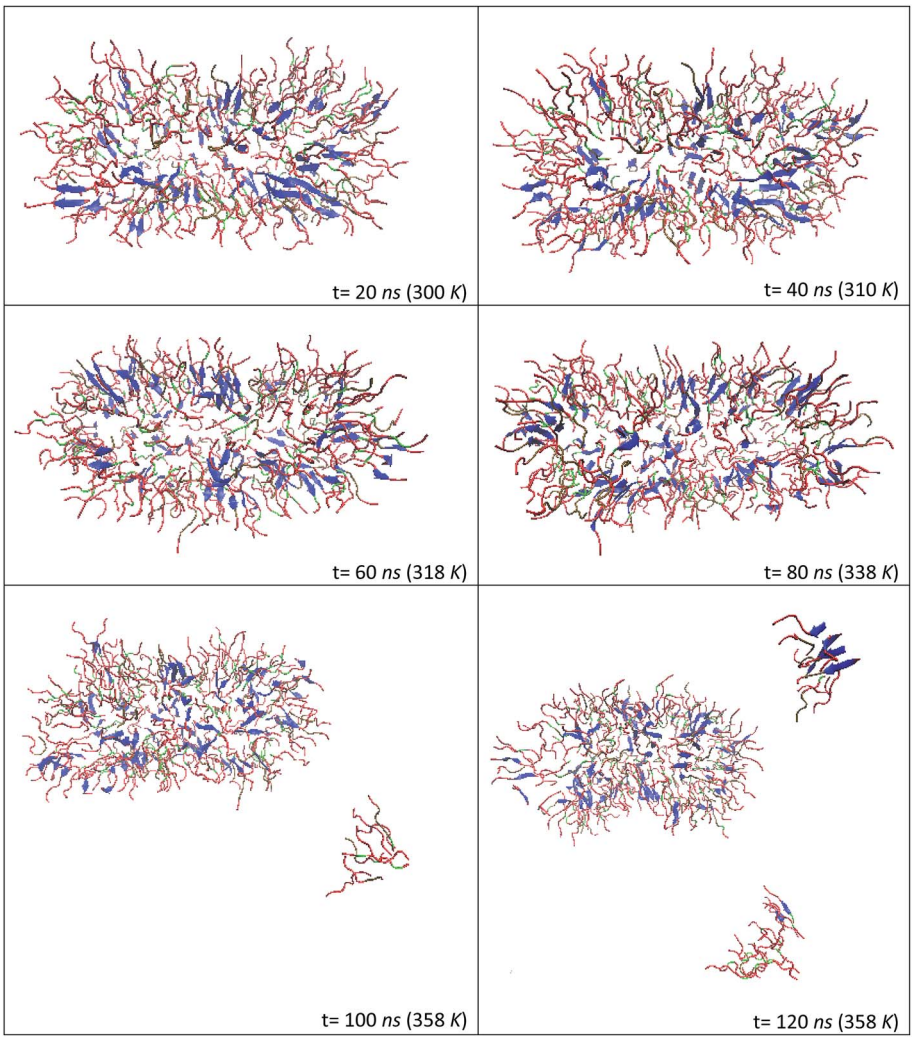


Fig. 8 Snapshots of the gradually heated PA1 nanofiber from 300 K to 358 K (simulation-2). Disassembly was observed to occur in the 100–120 ns interval which corresponds to 358 K.

"intermediate state" where the thermal energy provided is capable of disrupting the nanofiber structure but is not sufficient for the nanofiber to reach another stable configuration at the time periods tested. Indeed, the disassembly observed at 338 K was not present in a simulation of peptide nanofiber that was slowly (gradually) heated at 300 K, 310 K, 318 K, 338 K and 358 K for 20 ns each, (we also extended the simulation time by an additional 50 ns at 338 K) (see Fig. 7) suggesting that a slow transition into higher temperatures may increase the stability of the peptide backbone. As shown in Fig. 5, the simulation was started from a disassembled configuration at 338 K and heated it up to 358 K. The increased heat caused the nanofiber to reach a local minimum as a more stable state. The existence of intermediate states was previously shown experimentally by Tantakitti *et al.*,[15] who observed that competing interactions between repulsive and attractive forces can "lock" or "trap" supramolecular peptide nanosystems into thermodynamically unfavorable states, which are defined by local minima in the energy landscape of the system. In addition, movements between these minima have been shown to greatly alter the biological functions of a β-sheet forming peptide, with one state promoting cell survival and a second, metastable state, leading to cell death. The transient formation of an intermediate structure was also observed in simulations by Yu and Schatz,[46] who reported that the SLSLAAAGIKVAV PA sequence first assembles into a "pillar-like" form before assuming its final shape as a nanofiber.

Secondary structure analyses suggest that the peptide nanofibers predominantly exhibit random coil and secondly β-sheet structures, which is partially in agreement with Dagdas *et al.* and a characteristic feature of many peptide assemblies.[24] Valine and alanine residues in particular are β-sheet promoting amino acids, and the VVAG motif in the lauryl-VVAGERGD peptide is capable of mediating its self-assembly through β-sheet formation.[47] Minimal changes were observed between $Na^+$ and $Cl^-$-mediated assembly; however, the $Cl^-$-mediated assembly (the PA3 nanofiber) also had more β-sheet formation compared to the $Na^+$-mediated (the PA1 nanofiber)

 

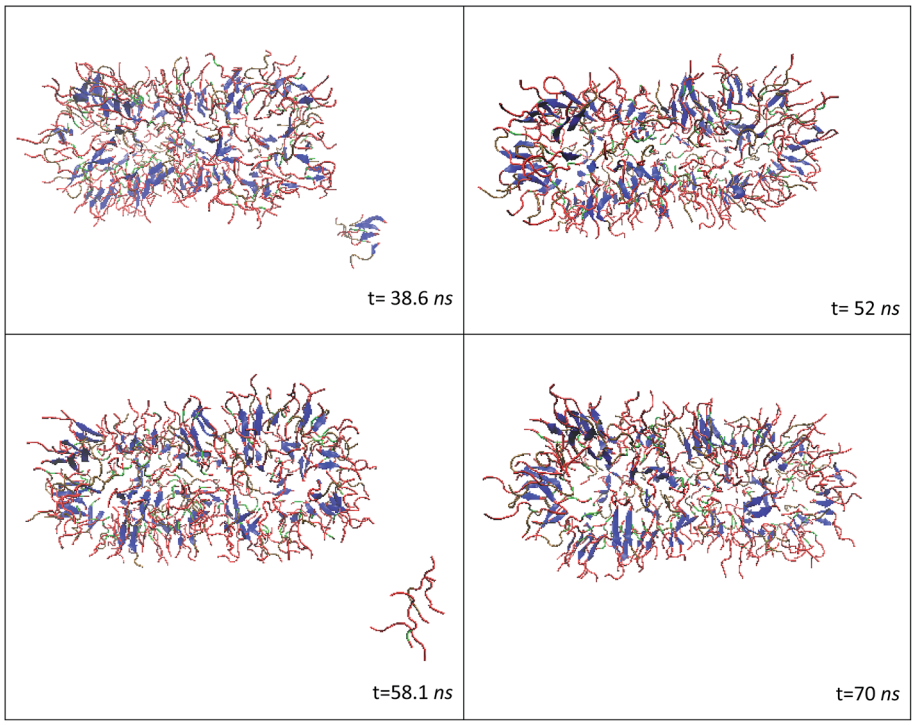


Fig. 9 Snapshots of PA2 nanofiber at 338 K. Although the nanofiber remained relatively intact, its radius and subunit configuration was unstable.

system, suggesting that pH change exhibits stronger effect on assembly behavior than does the inclusion of cations. Interestingly, secondary structure predictions were not strongly dependent on temperature, while Dagdas *et al.* observed that $Ca^{2+}$ and $Cl^{-}$-mediated assemblies react differently to temperature increases: $Ca^{2+}$-crosslinked nanofibers were relatively resistant to thermal stress up to 338 K, while HCl-treated nanofibers reacted immediately to temperature changes from 308 K onwards. The difference between these observations may result from the ability of small assemblies to still retain their secondary organization despite the disassembly of the nanofibrous peptide network, which would affect CD measurements (as CD spectra are sensitive to mesoscale aggregate effects) but not MD simulations.[48] Our

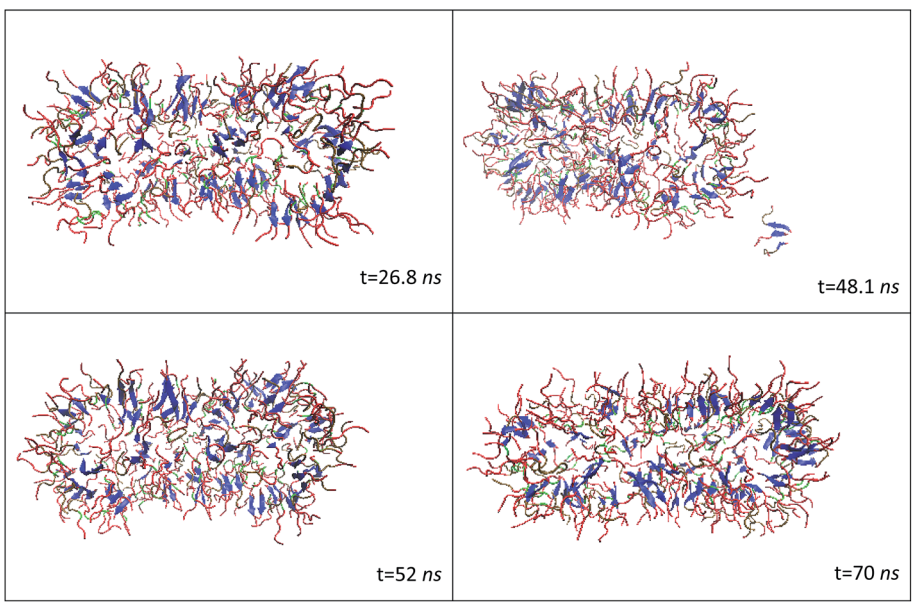


Fig. 10 Snapshots of the PA2 nanofiber at 358 K. The structure was generally able to retain its structural integrity, although slight fluctuations existed around 48 ns.

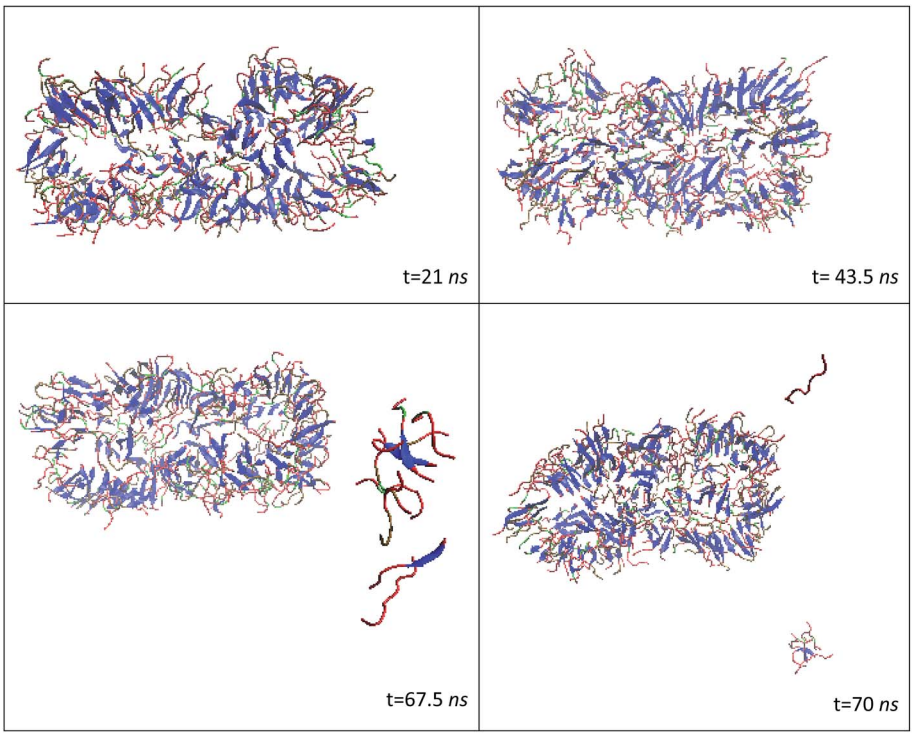


Fig. 11 Snapshots of PA3 nanofiber at 338 K; while the structure was generally stable, small peptide fragments were observed to leave the peptide structure towards the end of the simulation period.

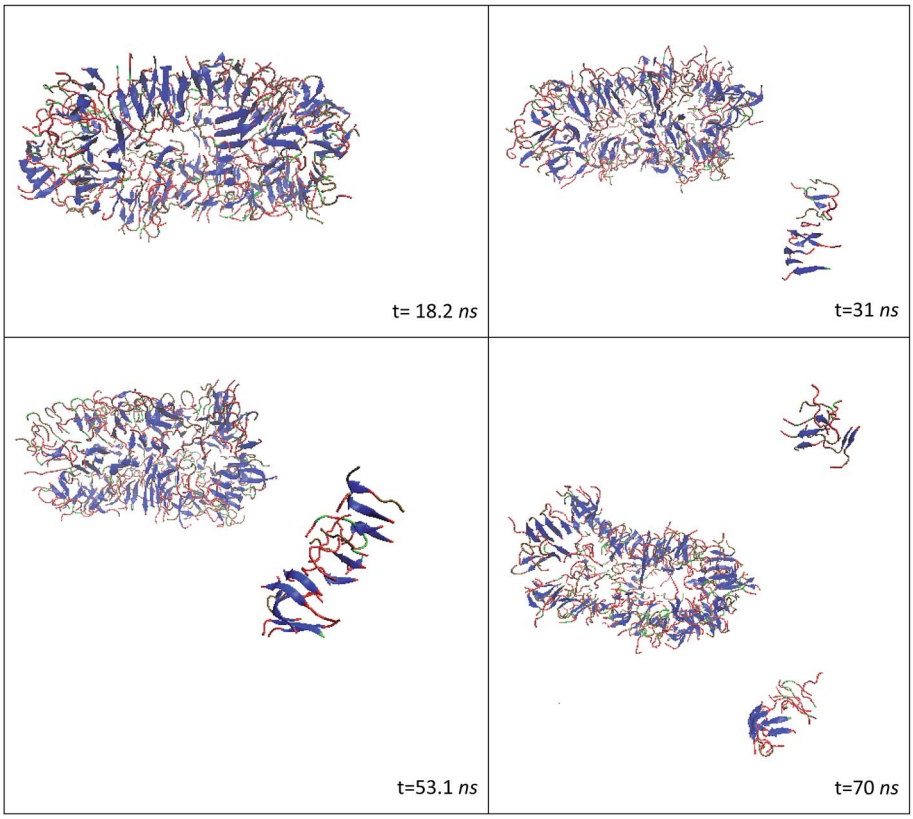


Fig. 12 Snapshots of PA3 nanofiber at 358 K. The nanofiber was much less stable compared to 338 K results, and the structure rapidly split into three sections.

 

Table 1 Percentage of β-sheet and random coil conformations

| | 300 K | 310 K | 318 K | 338 K | 358 K |
|---|---|---|---|---|---|
| **PA1 nanofiber** | | | | | |
| β-Sheet (coil) | 9% (69%) | 11% (66%) | 11% (66%) | **9% (disintegration)** (66%) | 10% (65%) |
| **PA2 nanofiber** | | | | | |
| β-Sheet (coil) | 10% (67%) | **9% (disintegration)** (67%) | 11% (65%) | 10% (65%) | 11% (63%) |
| **PA3 nanofiber** | | | | | |
| β-Sheet (coil) | 15% (59%) | 18% (57%) | 18% (55%) | 21% (53%) | **19% (disintegration)** (54%) |

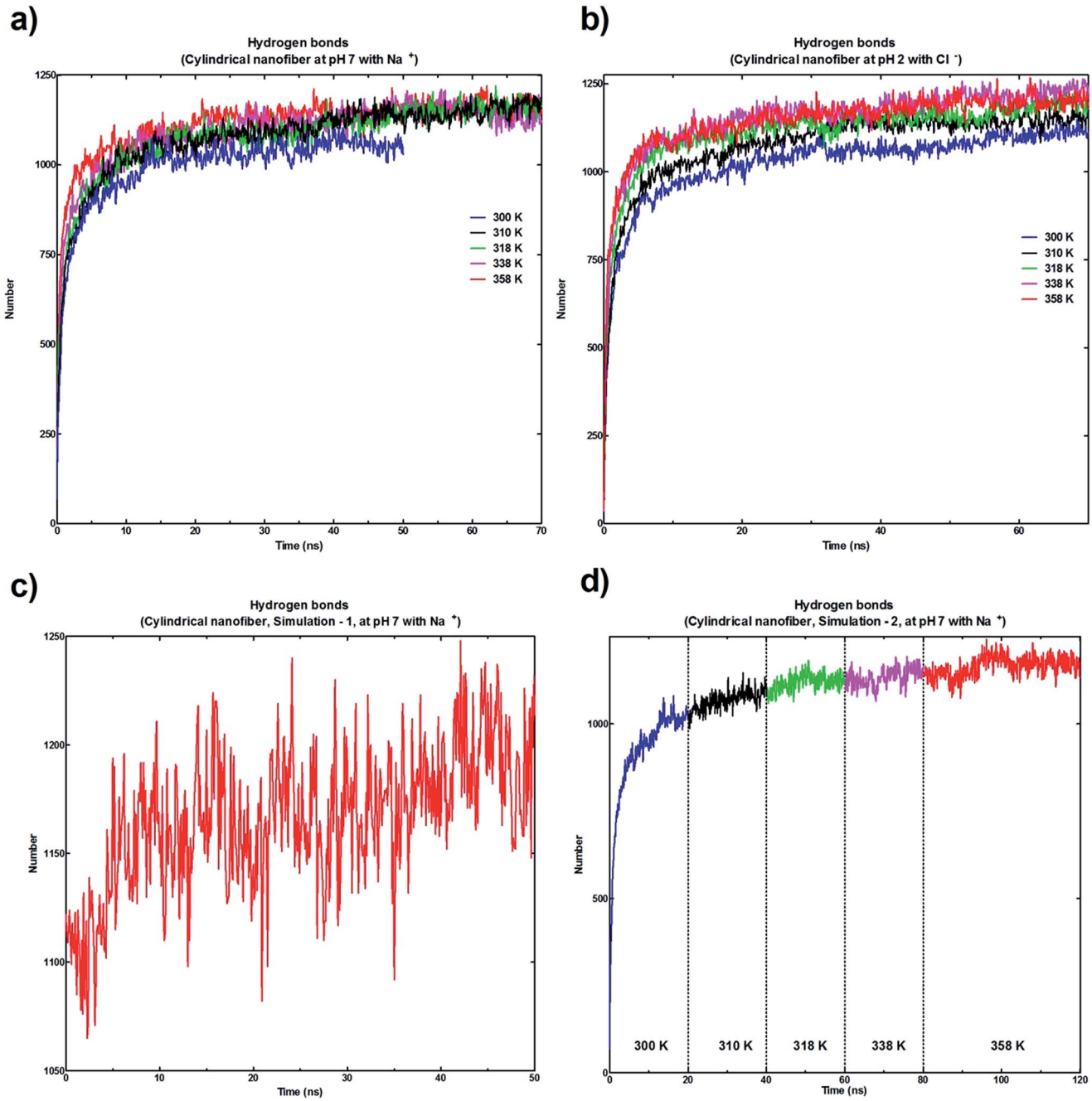


Fig. 13 Number of H-bonds formed between PA molecules as a function of simulation time. H-bondings were observed to increase with temperature, but did not differ considerably between the three PA systems tested. (a) PA1 nanofiber, (b) PA3 nanofiber, (c) simulation-1, (d) simulation-2.

results therefore confirm that the temperature-dependent changes in Dagdas *et al.*'s CD spectra are not from the interactions within individual nanofiber units, but possibly from the disassembly of nanofiber bundles, truncation of nanofiber length and other mesoscale structural effects that may contribute to CD signals. Differences between the behaviors of macro- and microscale assemblies were also proposed as the reason that Dagdas *et al.* observed relatively small changes in the oscillatory rheology of $Ca^{2+}$-crosslinked nanofibers, while a large loss of β-sheet signatures was present in their CD spectra at identical temperatures. Our simulation experiments introduce an additional layer of complexity to this model, suggesting that, even though the core nanofiber was intact until higher (338–358 K) temperatures, the overall nanofiber structure might be altered through temperature and the method by which the peptide hydrogel has been formed. In addition, small differences in the temperature responses of $Cl^-$, $Ca^{2+}$ and $Na^+$-crosslinked gels may play more important roles in biological systems, into which peptide hydrogels are frequently implanted.[49–51]

While we only investigated the changes that occur in response to temperature and pH changes, it is known that the biocompatibility and cell-recruiting, drug-encapsulating, immune system-inducing and differentiation-promoting capacities of PAs depend strongly on their structural properties.[3,52,53] For example, Moyer *et al.*[11] have shown that the location and length of the alkyl tail can drastically alter the morphology of pH-responsive, self-assembled peptide amphiphile systems, and that cylindrical nanofibers had around 7-fold higher encapsulation efficiency for camptothecin compared to spherical assemblies. In contrast, Mumcuoglu *et al.*[54] demonstrated that cell-penetrating peptide nanospheres were uptaken by the cells more compared to nanofibers because peptide nanofibers bound strongly to the cellular membrane and were internalized to a lesser degree by the cells. In addition, two lysine-rich peptides were shown by Newcomb *et al.*[55] to exhibit markedly different cytotoxic effects depending on their hydrogen bonding interactions, with the H-bond-rich β-sheet forming peptide showing minimal toxicity and the H-bond-poor sequence rapidly disrupting the integrity of both cell membranes and liposomes. As electrostatic interactions can greatly alter the macrostructure of the peptide system, it is possible that the gelation agent used for their self-assembly will play a role in determining their morphology and, consequently, effects in biological systems, which should be considered for the design of peptide systems for use in regenerative medicine.

## Conclusion

Here, we have shown that the stability of PA nanofibers under temperature changes depends heavily on the conditions used to precipitate the self-assembly process. In particular, the $Cl^-$-mediated assembly of the lauryl-VVAGERGD PA was reversed only at 358 K, while $Na^+$-mediated assembly experienced a loss in structure at 338 K but retained its organization at 358 K. While extended simulation times did not elicit any change in the organization of the PA1 nanofiber, the pattern of heating appeared to change the structural response of the self-assembled peptide amphiphile system: PA1 was observed to be stable at 358 K when heated directly to that temperature, but lost its morphology under a temperature ramp from 300 K to 358 K. In addition to the temperature and pH changes, counterion-based differences may also exist in factors such as mechanical elasticity, protease resistance and drug release capacity, which may be especially pronounced in the ion-rich environment experienced by PA gels used in *in vivo* therapeutic applications. As such, we believe the considerations outlined herein should be taken into account for the design and modeling of future peptide systems.

## Acknowledgements

The work was partially supported by TUBITAK grant no. 112T452. Numerical calculations reported in this paper were performed at TUBITAK ULAKBIM High Performance and Grid Computing Center (TRUBA resources).

## References

1 V. Tysseling-Mattiace, V. Sahni, K. Niece, D. Birch, C. Czeisler, M. Fehlings, S. Stupp and J. Kessler, Self-assembling nanofibers inhibit glial scar formation and promote axon elongation after spinal cord injury, *J. Neurosci.*, 2008, **28**(14), 3814–3823.

2 R. Ellis-Behnke, Y. Liang, S. You, D. Tay, S. Zhang, K. So and G. Schneider, Nano neuro knitting: peptide nanofiber scaffold for brain repair and axon regeneration with functional return of vision, *Proc. Natl. Acad. Sci. U. S. A.*, 2006, **103**(19), 7530.

3 G. Silva, C. Czeisler, K. Niece, E. Beniash, D. Harrington, J. Kessler and S. Stupp, Selective differentiation of neural progenitor cells by high-epitope density nanofibers, *Science*, 2004, **303**(5662), 1352–1355.

4 E. Arslan, I. C. Garip, G. Gulseren, A. B. Tekinay and M. O. Guler, Bioactive supramolecular Peptide nanofibers for regenerative medicine, *Adv. Healthcare Mater.*, 2014, **3**(9), 1357–1376.

5 J. Hartgerink, E. Beniash and S. Stupp, Self-assembly and mineralization of peptide-amphiphile nanofibers, *Science*, 2001, **294**(5547), 1684–1688.

6 J. Hartgerink, E. Beniash and S. Stupp, Peptide-amphiphile nanofibers: a versatile scaffold for the preparation of self-assembling materials, *Proc. Natl. Acad. Sci. U. S. A.*, 2002, **99**(8), 5133–5138.

7 D. Lowik, E. Leunissen, M. van den Heuvel, M. Hansen and J. van Hest, Stimulus responsive peptide based materials, *Chem. Soc. Rev.*, 2010, **39**(9), 3394–3412.

8 D. Lowik, T. Meijer and J. van Hest, Tuning secondary structure and self-assembly of amphiphilic peptides, *Biopolymers*, 2005, **80**(4), 597.

9 A. Dehsorkhi, V. Castelletto and I. Hamley, Self-assembling amphiphilic peptides, *J. Pept. Sci.*, 2014, **20**(7), 453–467.

 

10 M. Yu, T. Tang, A. Takasu and M. Higuchi, pH- and thermo-induced morphological changes of an amphiphilic peptide-grafted copolymer in solution, *Polym. J.*, 2014, **46**(1), 52–58.
11 T. Moyer, J. Finbloom, F. Chen, D. Toft, V. Cryns and S. Stupp, pH and Amphiphilic Structure Direct Supramolecular Behavior in Biofunctional Assemblies, *J. Am. Chem. Soc.*, 2014, **136**(42), 14746–14752.
12 S. Toksoz and M. Guler, Self-assembled peptidic nanostructures, *Nano Today*, 2009, **4**(6), 458–469.
13 J. Miravet, B. Escuder, M. Segarra-Maset, M. Tena-Solsona, I. Hamley, A. Dehsorkhi and V. Castelletto, Self-assembly of a peptide amphiphile: transition from nanotape fibrils to micelles, *Soft Matter*, 2013, **9**(13), 3558–3564.
14 R. da Silva, D. van der Zwaag, L. Albertazzi, S. Lee, E. Meijer and S. Stupp, Super-resolution microscopy reveals structural diversity in molecular exchange among peptide amphiphile nanofibres, *Nat. Commun.*, 2016, **7**, 11561.
15 F. Tantakitti, J. Boekhoven, X. Wang, R. Kazantsev, T. Yu, J. Li, E. Zhuang, R. Zandi, J. Ortony, C. Newcomb, L. Palmer, G. Shekhawat, M. de la Cruz, G. Schatz and S. Stupp, Energy landscapes and functions of supramolecular systems, *Nat. Mater.*, 2016, **15**(4), 469–476.
16 I. Hamley, A. Dehsorkhi, V. Castelletto, S. Furzeland, D. Atkins, J. Seitsonen and J. Ruokolainen, Reversible helical unwinding transition of a self-assembling peptide amphiphile, *Soft Matter*, 2013, **9**(39), 9290–9293.
17 K. Niece, J. Hartgerink, J. Donners and S. Stupp, Self-assembly combining two bioactive peptide-amphiphile molecules into nanofibers by electrostatic attraction, *J. Am. Chem. Soc.*, 2003, **125**(24), 7146–7147.
18 S. Toksoz, R. Mammadov, A. Tekinay and M. Guler, Electrostatic effects on nanofiber formation of self-assembling peptide amphiphiles, *J. Colloid Interface Sci.*, 2011, **356**(1), 131–137.
19 Y. Chen, H. Gan and Y. Tong, pH-Controlled Hierarchical Self-Assembly of Peptide Amphiphile, *Macromolecules*, 2015, **48**(8), 2647–2653.
20 A. Ghosh, M. Haverick, K. Stump, X. Yang, M. Tweedle and J. Goldberger, Fine-Tuning the pH Trigger of Self-Assembly, *J. Am. Chem. Soc.*, 2012, **134**(8), 3647–3650.
21 A. Dehsorkhi, V. Castelletto, I. Hamley, J. Adamcik and R. Mezzenga, The effect of pH on the self-assembly of a collagen derived peptide amphiphile, *Soft Matter*, 2013, **9**(26), 6033–6036.
22 M. Deng, D. Yu, Y. Hou and Y. Wang, Self-assembly of Peptide-Amphiphile C-12-A beta (11-17) into Nanofibrils, *J. Phys. Chem. B*, 2009, **113**(25), 8539–8544.
23 H. Guo, J. Zhang, T. Xu, Z. Zhang, J. Yao and Z. Shao, The Robust Hydrogel Hierarchically Assembled from a pH Sensitive Peptide Amphiphile Based on Silk Fibroin, *Biomacromolecules*, 2013, **14**(8), 2733–2738.
24 Y. Dagdas, A. Tombuloglu, A. Tekinay, A. Dana and M. Guler, Interfiber interactions alter the stiffness of gels formed by supramolecular self-assembled nanofibers, *Soft Matter*, 2011, **7**(7), 3524–3532.
25 Y. Cote, I. Fu, E. Dobson, J. Goldberger, H. Nguyen and J. Shen, Mechanism of the pH-Controlled Self-Assembly of Nanofibers from Peptide Amphiphiles, *J. Phys. Chem. C*, 2014, **118**(29), 16272–16278.
26 I. Fu, C. Markegard, B. Chu and H. Nguyen, Role of Hydrophobicity on Self-Assembly by Peptide Amphiphiles *via* Molecular Dynamics Simulations, *Langmuir*, 2014, **30**(26), 7745–7754.
27 I. Fu, C. Markegard, B. Chu and H. Nguyen, The Role of Electrostatics and Temperature on Morphological Transitions of Hydrogel Nanostructures Self-Assembled by Peptide Amphiphiles Via Molecular Dynamics Simulations, *Adv. Healthcare Mater.*, 2013, **2**(10), 1388–1400.
28 E. Tekin, Molecular dynamics simulations of self-assembled peptide amphiphile based cylindrical nanofibers, *RSC Adv.*, 2015, **5**(82), 66582–66590.
29 E. Tekin, Odd-even effect in the potential energy of the self-assembled peptide amphiphiles, *Chem. Phys. Lett.*, 2014, **614**, 204–206.
30 E. Pashuck, H. Cui and S. Stupp, Tuning Supramolecular Rigidity of Peptide Fibers through Molecular Structure, *J. Am. Chem. Soc.*, 2010, **132**(17), 6041–6046.
31 P. Smith and W. Vangunsteren, The viscosity of SPC and SPC/E water at 277-K and 300-K, *Chem. Phys. Lett.*, 1993, **215**(4), 315–318.
32 B. Hess, C. Kutzner, D. van der Spoel and E. Lindahl, GROMACS 4: algorithms for highly efficient, load-balanced, and scalable molecular simulation, *J. Chem. Theory Comput.*, 2008, **4**(3), 435–447.
33 C. Oostenbrink, A. Villa, A. Mark and W. Van Gunsteren, A biomolecular force field based on the free enthalpy of hydration and solvation: the GROMOS force-field parameter sets 53A5 and 53A6, *J. Comput. Chem.*, 2004, **25**(13), 1656–1676.
34 O. Berger, O. Edholm and F. Jahnig, Molecular dynamics simulations of a fluid bilayer of dipalmitoylphosphatidylcholine at full hydration, constant pressure, and constant temperature, *Biophys. J.*, 1997, **72**(5), 2002–2013.
35 B. Hess, H. Bekker, H. Berendsen and J. Fraaije, LINCS: a linear constraint solver for molecular simulations, *J. Comput. Chem.*, 1997, **18**(12), 1463–1472.
36 T. Darden, D. York and L. Pedersen, Particle mesh Ewald – an $n\log(n)$ method for Ewald sums in large systems, *J. Chem. Phys.*, 1993, **98**(12), 10089–10092.
37 G. Bussi, D. Donadio and M. Parrinello, Canonical sampling through velocity rescaling, *J. Chem. Phys.*, 2007, **126**(1), 014101–014107.
38 M. Parrinello and A. Rahman, Polymorphic transitions in single-crystals – a new molecular-dynamics method, *J. Appl. Phys.*, 1981, **52**(12), 7182–7190.
39 W. Humphrey, A. Dalke and K. Schulten, VMD: visual molecular dynamics, *J. Mol. Graphics Modell.*, 1996, **14**(1), 33–38.
40 P. Li, B. P. Roberts, D. K. Chakravorty and K. M. Merz, Rational Design of Particle Mesh Ewald Compatible Lennard-Jones Parameters for +2 Metal Cations in Explicit Solvent, *J. Chem. Theory Comput.*, 2013, **9**(6), 2733–2748.
41 P. Li and K. M. Merz, Taking into Account the Ion-induced Dipole Interaction in the Nonbonded Model of Ions, *J. Chem. Theory Comput.*, 2014, **10**(1), 289–297.

42 S. Mamatkulov, M. Fyta and R. Netz, Force fields for divalent cations based on single-ion and ion-pair properties, *J. Chem. Phys.*, 2013, **138**(2), 024505.
43 C. Bergonzo, K. B. Hall and T. E. Cheatham, Divalent Ion Dependent Conformational Changes in an RNA Stem-Loop Observed by Molecular Dynamics, *J. Chem. Theory Comput.*, 2016, **12**(7), 3382–3389.
44 W. Kabsch and C. Sander, Dictionary of protein secondary structure – pattern-recognition of hydrogen-bonded and geometrical features, *Biopolymers*, 1983, **22**(12), 2577–2637.
45 T. Creighton, Protein folding, *Biochem. J.*, 1990, **270**(1), 1–16.
46 T. Yu and G. Schatz, Free-Energy Landscape for Peptide Amphiphile Self-Assembly: Stepwise *versus* Continuous Assembly Mechanisms, *J. Phys. Chem. B*, 2013, **117**(45), 14059–14064.
47 R. Garifullin and M. Guler, Supramolecular chirality in self-assembled peptide amphiphile nanostructures, *Chem. Commun.*, 2015, **51**(62), 12470–12473.
48 K. Rajagopal and J. Schneider, Self-assembling peptides and proteins for nanotechnological applications, *Curr. Opin. Struct. Biol.*, 2004, **14**(4), 480–486.
49 S. Ghanaati, M. Webber, R. Unger, C. Orth, J. Hulvat, S. Kiehna, M. Barbeck, A. Rasic, S. Stupp and C. Kirkpatrick, Dynamic *in vivo* biocompatibility of angiogenic peptide amphiphile nanofibers, *Biomaterials*, 2009, **30**(31), 6202–6212.
50 S. Standley, D. Toft, H. Cheng, S. Soukasene, J. Chen, S. Raja, V. Band, H. Band, V. Cryns and S. Stupp, Induction of Cancer Cell Death by Self-assembling Nanostructures Incorporating a Cytotoxic Peptide, *Cancer Res.*, 2010, **70**(8), 3020–3026.
51 M. Webber, J. Tongers, M. Renault, J. Roncalli, D. Losordo and S. Stupp, Development of bioactive peptide amphiphiles for therapeutic cell delivery, *Acta Biomater.*, 2010, **6**(1), 3–11.
52 M. Guler, S. Soukasene, J. Hulvat and S. Stupp, Presentation and recognition of biotin on nanofibers formed by branched peptide amphiphiles, *Nano Lett.*, 2005, **5**(2), 249–252.
53 H. Liu, K. Moynihan, Y. Zheng, G. Szeto, A. Li, B. Huang, D. Van Egeren, C. Park and D. Irvine, Structure-based programming of lymph-node targeting in molecular vaccines, *Nature*, 2014, **507**(7493), 519–522.
54 D. Mumcuoglu, M. Sardan, T. Tekinay, M. Guler and A. Tekinay, Oligonucleotide Delivery with Cell Surface Binding and Cell Penetrating Peptide Amphiphile Nanospheres, *Mol. Pharm.*, 2015, **12**(5), 1584–1591.
55 C. J. Newcomb, S. Sur, J. H. Ortony, O. S. Lee, J. B. Matson, J. Boekhoven, J. M. Yu, G. C. Schatz and S. I. Stupp, Cell death *versus* cell survival instructed by supramolecular cohesion of nanostructures, *Nat. Commun.*, 2014, **5**, 3321.